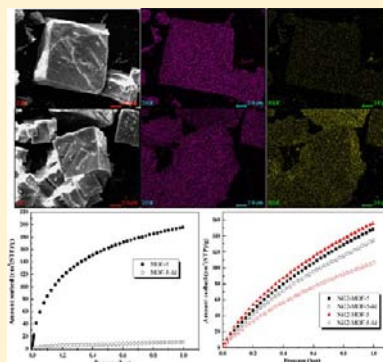


Enhanced Hydrostability in Ni-Doped MOF-5

Huanhuan Li, Wei Shi,* Kaina Zhao, Han Li, Yanmin Bing, and Peng Cheng*

Department of Chemistry and Key Laboratory of Advanced Energy Materials Chemistry (MOE), and TKL of Metal and Molecule Based Material Chemistry, Nankai University, Tianjin 300071, P. R. China

ABSTRACT: Ni-doped MOF-5s were successfully synthesized for the first time via solvothermal crystallization process to enhance the hydrostability. Several characterization techniques, including X-ray diffraction (XRD), thermogravimetric analysis (TGA), scanning electron microscopy (SEM), energy-dispersive spectroscopy instrument (EDS), inductively coupled plasma (ICP), infrared spectroscopy (IR), atomic sorption, diffuse-reflectance UV–vis spectroscopy, and gas sorption measurement, strongly support the effective incorporation of Ni(II) ions into the framework. The results demonstrated that the Ni-doped MOF-5s not only exhibit larger Langmuir specific surface areas and larger pores than the undoped MOF-5, but also significantly enhance water resistance of the framework. The H₂ uptake capacity of undoped MOF-5 drops rapidly when exposed to the ambient air, whereas the H₂ adsorptions of the Ni-doped MOF-5s remain stable for 4 days.



INTRODUCTION

Energy issues and environmental concerns have generated great attention for hydrogen as a transportation fuel. To make this source of energy economically viable, a high-performance hydrogen storage system is widely recognized as a critical element.^{1,2} Whereas hydrogen for transportation applications is currently stored using cryogenics or high pressure, there is a lot of research interest to develop new hydrogen storage materials. However, the multiple-target criteria for the successful implementation of such storage materials have not yet been met.

Over the past decade, metal–organic frameworks (MOFs), as highly porous crystalline materials constructed by coordination bonds between metal ions/clusters and organic ligands, have developed very fast due to not only their intriguing structures but also the potential applications,³ such as gas separation and storage,^{4,5} catalysis, and sensing.^{6,7} MOF-5 is one of the most prominent representatives of these porous materials. It consists of four [Zn₄O]⁶⁺ clusters in octahedral subunits that are connected to each other by benzene-1,4-dicarboxylate (BDC) groups, to form a porous cubic framework.⁸ This special structure gives large surface area, exceptional pore volume, and relatively high thermal stability to MOF-5. Although MOF-5 displays considerable applications in many fields, the most attractive property is the hydrogen storage at low temperature and moderate pressures.⁹ MOF-5 can adsorb 7.1 wt % excess H₂ at 77 K with pressure up to 40 bar, while the total hydrogen uptake of MOF-5 could reach up to 10 wt % at 100 bar, corresponding to a record volumetric storage density of 66 g L⁻¹.¹⁰ The H₂ uptake of MOF-5 is competitive not only in the MOF family but also in all of the hydrogen storage materials. However, MOF-5 is moisture-sensitive even under atmospheric conditions, because the metal–oxygen coordination bond is relative weak, which allows for the attack by water molecules, resulting in the phase

transformation and structure collapse.¹¹ Hence, development of a new method to enhance the hydrostability of MOFs has become a challenge for chemists.

To date, there are only a few works reported on the enhancement of hydrostability for MOF-5.^{12,13} Dingemans and co-workers found that MOF-5 materials were significantly less sensitive to water without impairing the hydrogen uptake capacity by simply introducing one or two hydrophobic methyl functionalities on the BDC moiety.¹² Park and co-workers successfully synthesized a novel hybrid composite CNT@MOF-5 to increase the hydrostability.¹³ These results show that the modified ligand with other groups or combined MOF-5 with other gas storage materials are both feasible ways to enhance the hydrostability of MOF-5. In this work, we explored a new way for improving the hydrostability of MOF-5 by doping Ni(II) ions into the framework during the crystallization process. Moreover, it was found that Ni-doped MOF-5s exhibited not only higher specific surface areas (SSA) and larger pores, but also enhanced hydrostability toward ambient moisture compared to the undoped MOF-5.

EXPERIMENTAL SECTION

Materials. All chemicals were purchased from commercial suppliers and were used without further purification.

Synthesis. *Synthesis of MOF-5.* Pure MOF-5 was prepared according to a previously reported method,¹⁴ and the original synthesis procedure was modified. Zn(NO₃)₂·6H₂O (0.149 g, 0.5 mmol) and 1,4-benzenedicarboxylic acid (H₂BDC) (0.0166 g, 0.1 mmol) were dissolved in 15 mL of *N,N*-dimethylformamide (DMF) at room temperature. The mixture was transferred into a 25 mL Teflon-lined autoclave, which was sealed and maintained at 120 °C for 21 h to yield large, cube-shaped crystals of MOF-5. The reaction vessel was then

Received: February 8, 2012

Published: August 17, 2012

removed from the oven and allowed to cool to room temperature. The obtained cubic crystals were washed with DMF.

Synthesis of Ni-Doped MOF-5s. The synthesis of Ni-doped MOF-5s was performed following a similar procedure of MOF-5 as described above, in which mixed $\text{Ni}(\text{NO}_3)_2 \cdot 6\text{H}_2\text{O}$ and $\text{Zn}(\text{NO}_3)_2 \cdot 6\text{H}_2\text{O}$ (0.05 mmol $\text{Ni}(\text{NO}_3)_2 \cdot 6\text{H}_2\text{O}$ and 0.45 mmol $\text{Zn}(\text{NO}_3)_2 \cdot 6\text{H}_2\text{O}$ for Ni13-MOF-5; 0.25 mmol $\text{Ni}(\text{NO}_3)_2 \cdot 6\text{H}_2\text{O}$ and 0.25 mmol $\text{Zn}(\text{NO}_3)_2 \cdot 6\text{H}_2\text{O}$ for Ni22-MOF-5) took the place of pure $\text{Zn}(\text{NO}_3)_2 \cdot 6\text{H}_2\text{O}$. Light green cube-shaped crystals of Ni13-MOF-5 and Ni22-MOF-5 were obtained after being washed with DMF several times, respectively.

The chemical composition of the two Ni-doped MOF-5s was determined by inductively coupled plasma (ICP), and evidenced by energy-dispersive X-ray spectroscopy (EDS), atomic absorption spectroscopy (AAS), and elemental analysis (Table 1), resulting in

Table 1. Metal Ion Content Analysis for Ni-Doped MOF-5s

samples	ICP	EDS	AAS
Ni13-MOF-5	Ni 13.0%	Ni 13.0%	Ni 12.4%
Ni13-MOF-5	Zn 87.0%	Zn 87.0%	Zn 87.6%
Ni22-MOF-5	Ni 21.8%	Ni 24.8%	Ni 22.0%
Ni22-MOF-5	Zn 78.2%	Zn 75.2%	Zn 78.0%

the following materials: (a) $\text{Zn}_{3.48}\text{Ni}_{0.52}\text{O}(\text{BDC})_3(\text{DMF})_{2.6}$ (sample Ni13-MOF-5) with a yield of 66% based on BDC, containing 13% Ni and 87% Zn. Anal. Calcd (%): C, 39.93%; H, 3.18%; N, 3.80%. Found (%): C, 39.61%; H, 3.51%; N, 3.92%. (b) $\text{Zn}_{3.52}\text{Ni}_{0.88}\text{O}(\text{BDC})_3(\text{DMF})_{2.2}$ (sample Ni22-MOF-5) with a yield of 50%, comprising 22% Ni and 78% Zn. Anal. Calcd (%): C, 38.65%; H, 2.90%; N, 3.24%. Found (%): C, 38.27%; H, 3.38%; N, 3.22%.

Characterization. Powder X-ray diffraction (PXRD) patterns were recorded on a D/Max-2500 X-ray diffractometer using $\text{Cu K}\alpha$ radiation. The simulated powder patterns were calculated using Mercury 2.0. The purity and homogeneity of the bulk products were

determined by comparison of the simulated and experimental X-ray powder diffraction patterns.

Diffuse-reflectance UV–vis (DRUV–vis) spectra were recorded on a Jasco V-570 spectrophotometer equipped with a diffuse reflectance accessory in the wavelength range 300–900 nm. Thermogravimetric analyses (TGA) were performed on a Labsys NETZSCH TG 209 Setaram apparatus with a heating rate of 10 °C/min in the nitrogen atmosphere. Scanning electron microscope (SEM) images were measured on a Hitachi S-3500N equipped with an energy-dispersive X-ray spectroscopy (EDS) instrument. ICP was measured by ICP-9000(N+M) (USA Thermo Jarrell-Ash Corp). Atomic absorption spectroscopy was determined on HITACH 180-80. Elemental analyses (C, H, and N) were performed on a Perkin-Elmer 240 CHN elemental analyzer. Infrared spectroscopy (IR) spectra were recorded in the range 400–4000 cm^{-1} on a Bruker TENOR 27 spectrophotometer using KBr pellet.

All gas adsorption experiments were performed on a gas adsorption analyzer Autosorb-IQ2 (Quantachrome Instruments). Ultra-high purity N_2 , Ar, and H_2 were used in the adsorption study. Before measurements, the as-prepared MOFs were immersed in CHCl_3 for one week and then degassed at 120 °C for 12 h on degassing station. The degassed sample and sample cell were weighed precisely again and then transferred back to the analyzer. Large bulb cells (9 mm, from Quantachrome) of a known weight were loaded with degassed samples of ca. 90–100 mg were used for gas-sorption measurements, and the weight of each sample was recorded before and after degassing to confirm the removal of guest molecules.

The temperature of each sample for N_2 , H_2 , and Ar adsorption experiments was controlled by a refrigerated bath of either liquid nitrogen (77 K) or liquid argon (87 K). The N_2 and Ar sorption isotherms were recorded in the pressure range from 10^{-7} to 1 bar at 77 and 87 K, respectively. The H_2 sorption isotherms were carried out at 77 and 87 K with pressures ranging from 10^{-3} to 1 bar. Nonlocal density functional theory (NLDFT) pore size distributions were determined using the cylindrical pore model.

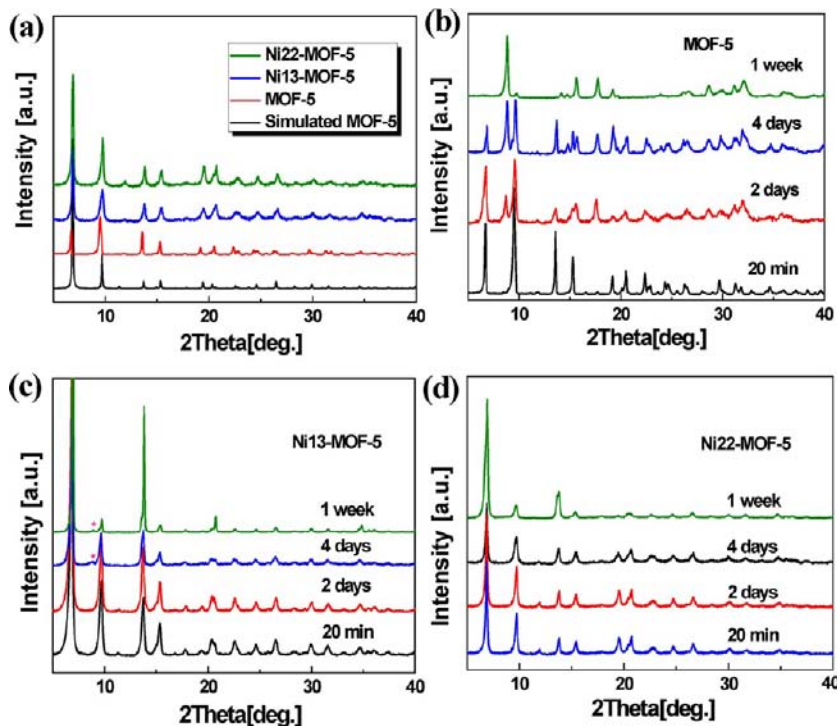


Figure 1. (a) PXRD patterns of as synthesized MOF-5, Ni13-MOF-5, Ni22-MOF-5, and the simulated MOF-5. (b) PXRD patterns of MOF-5. (c) PXRD patterns of Ni13-MOF-5. (d) PXRD patterns of Ni22-MOF-5. Parts b–d show the patterns change of exposed to static air conditions (25 °C and 30–37% relative humidity) for twenty minutes, two days, four days, and one week.

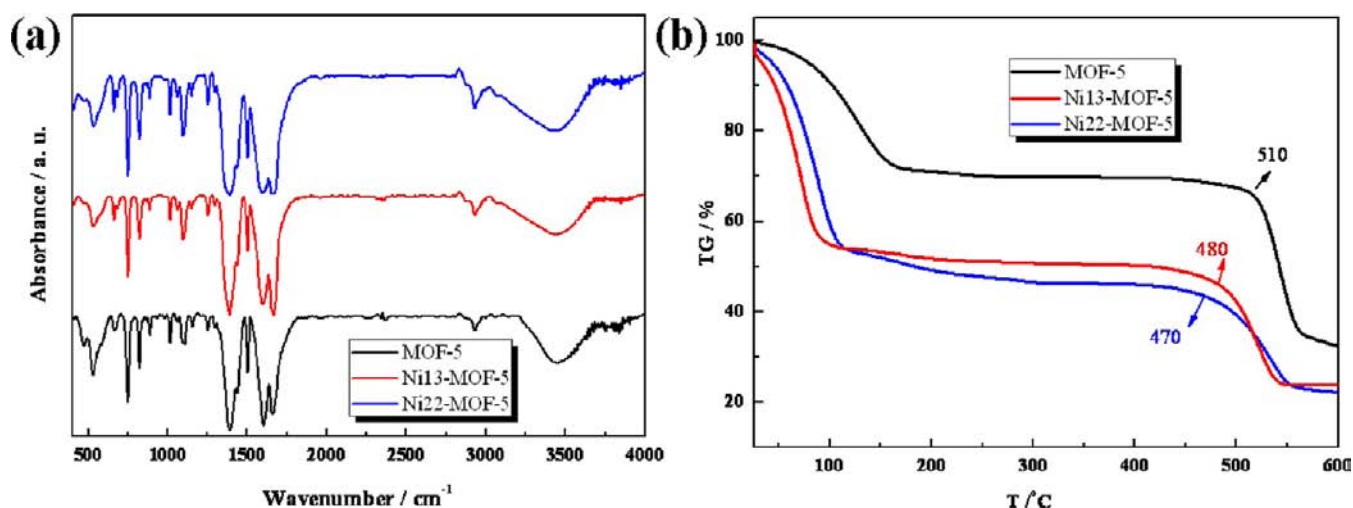


Figure 2. (a) Analogous IR spectra of MOF-5 and its Ni-doped products (Ni13-MOF-5 and Ni22-MOF-5). (b) TGA plot of the as-synthesized pure MOF-5, Ni13-MOF-5, and Ni22-MOF-5.

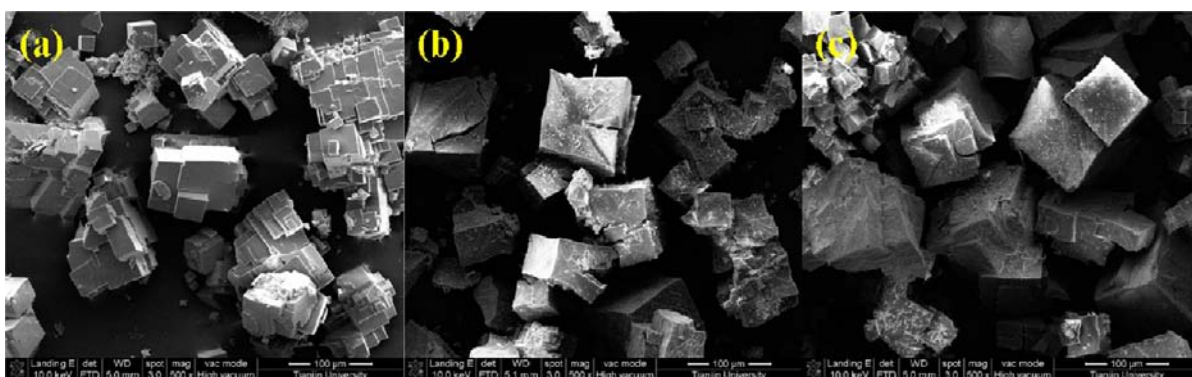


Figure 3. SEM images of (a) pure MOF-5, (b) Ni13-MOF-5, and (c) Ni22-MOF-5 crystals.

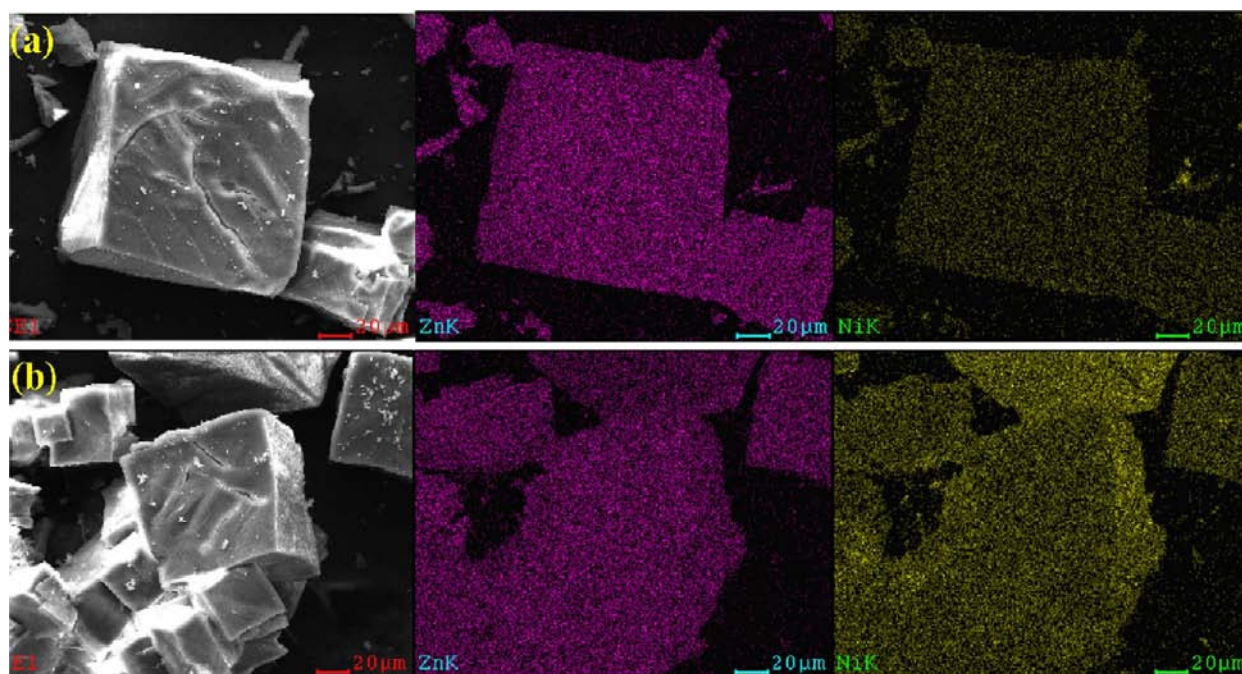


Figure 4. (a) EDS mapping of Ni13-MOF-5. (b) EDS mapping of Ni22-MOF-5. SEM image (left) and the corresponding elemental distributions of Zn (middle) and Ni (right). Scale bar: 20 μm .

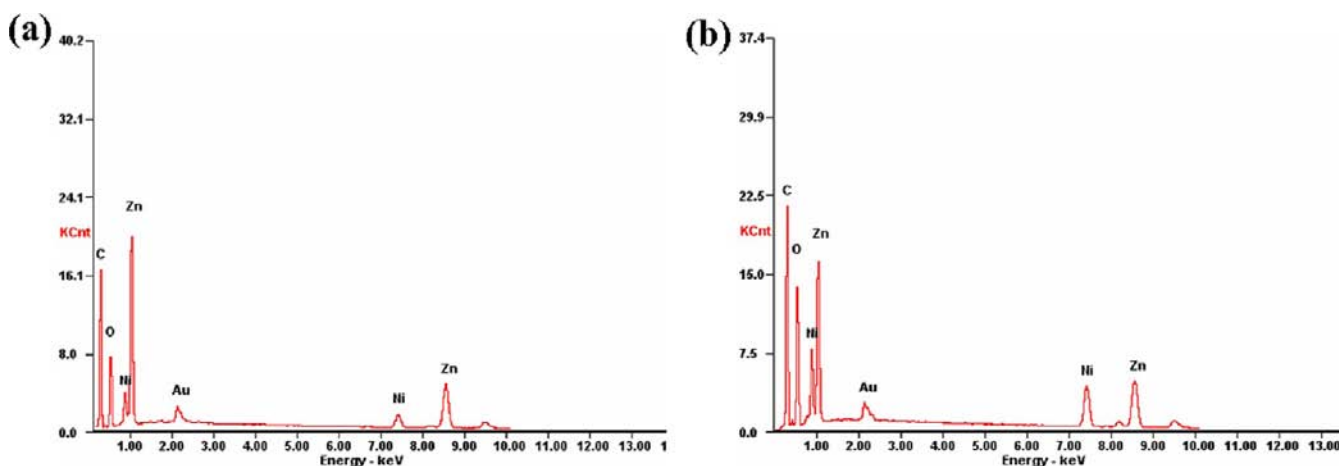


Figure 5. (a) EDS plots measured scanning the crystal of Ni13-MOF-5. (b) EDS plots measured scanning the crystal of Ni22-MOF-5.

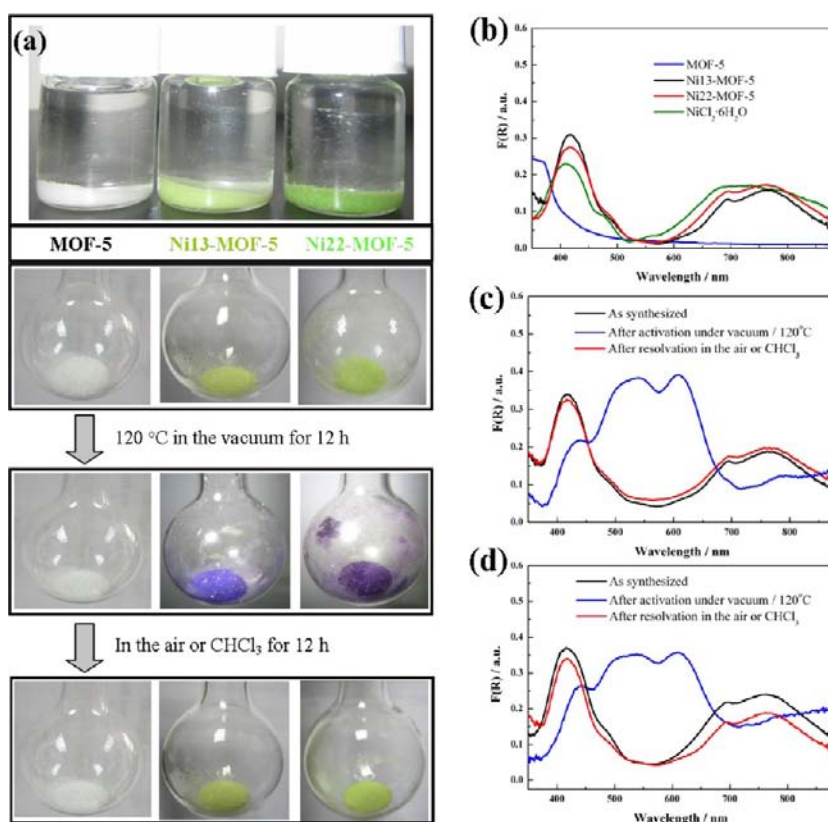


Figure 6. (a) Pictures of the color changes after evacuated in vacuum for 12 h and re-exposure to the air or CHCl_3 for MOF-5, Ni13-MOF-5, and Ni22-MOF-5. (b) DRUV-vis spectra of MOF-5, Ni13-MOF-5, and Ni22-MOF-5. (c) DRUV-vis spectra of Ni13-MOF-5. (d) DRUV-vis spectra of Ni22-MOF-5.

RESULTS AND DISCUSSION

PXRD Patterns of the Samples. The structures of the Ni-doped MOF-5s were confirmed to be isostructural to MOF-5 by the powder X-ray diffraction (PXRD), as shown in Figure 1a. The data present a unique crystalline phase, which is in good agreement with the simulated patterns from the single crystal data.^{9a} The pure phase of Ni-doped MOF-5s also suggests that the doped Ni(II) ions should be well incorporated into the framework and substitute partial Zn(II) ions of the $[\text{Zn}_4\text{O}]^{6+}$ clusters, as well as be observed in the Co-doped MOF-5.¹⁵ An interesting feature was found: Ni-doping greatly enhanced the hydrostability of MOF-5s when they were

exposed to ambient air (relative humidity: 30–37%) for different times, checked by PXRD (Figure 1b–d). For MOF-5, an extra peak at $2\theta = 8.82^\circ$ appears in two days (Figure 1b), indicating the decomposition of the framework.¹⁰ Subsequently, when exposed to moisture in air the relative intensity of the peak rapidly enhances, showing acceleration of the decomposition. After one week of exposure to moisture in air, no diffraction peaks belongs to MOF-5 can be observed, suggesting the complete transformation of the structure to $\text{ZnBDC}\cdot x\text{H}_2\text{O}$.^{10,16} The decomposition of Ni13-MOF-5 is much slower than that of pure MOF-5, as indicated by the appearance of the diffraction peak at $2\theta = 8.82^\circ$ which was

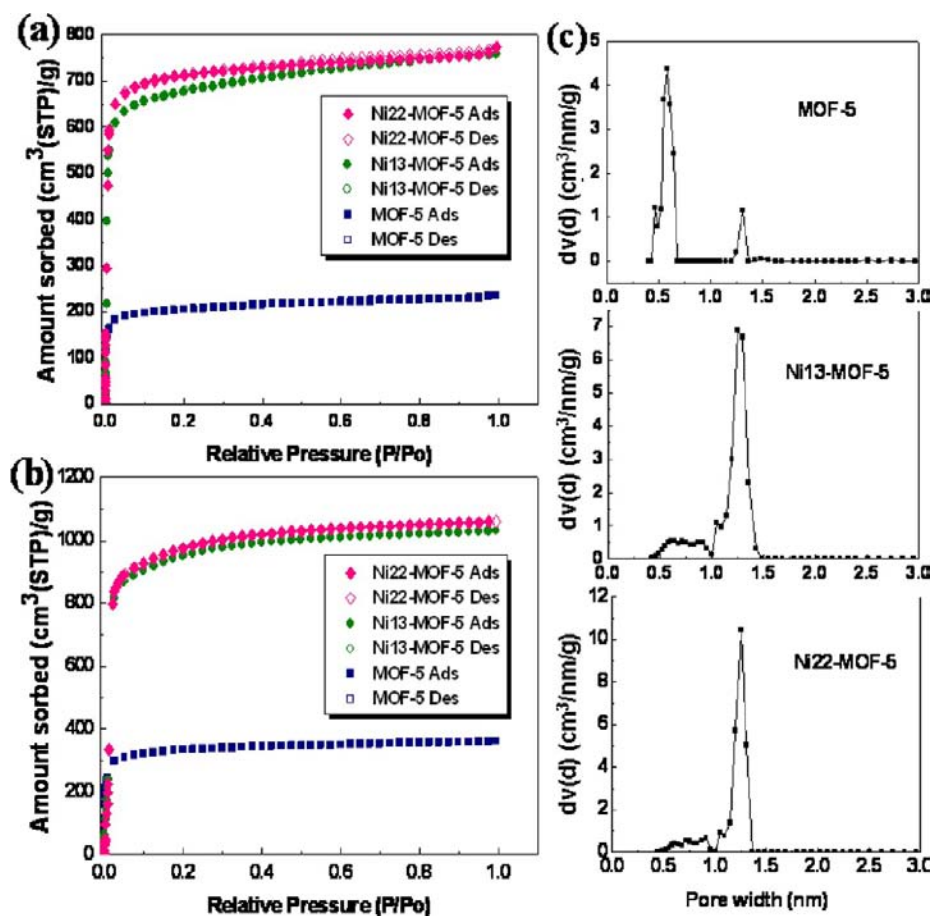


Figure 7. (a) Nitrogen and (b) argon sorption isotherms of MOF-5 and Ni-doped MOF-5s at 77 and 87 K, respectively. (c) Pore size distributions from Ar adsorption at 87 K calculated by NLDFT methods.

observed after four days of exposure to air (Figure 1c). Even after one week, the main peaks belonging to MOF-5 structure still exist. The diffraction peak at $2\theta = 8.82^\circ$ was not observed even after one week for Ni22-MOF-5, indicating higher hydrostability (Figure 1d).

IR and TGA of the Samples. The IR spectra of the undoped and Ni-doped MOF-5s are almost the same, further confirming the isostructure (Figure 2a).

Thermogravimetric analysis (TGA) curves of MOF-5 and Ni-doped MOF-5s all display two main steps of weight loss (Figure 2b). The first step of weight loss in the temperature range 30–150 °C can be attributed to the loss of guest molecules. The second step is due to the decomposition of organic linkers. Compared to that of pure MOF-5, the second weight loss of Ni-doped MOF-5s occurs in lower temperature. The behavior also indicates that Ni(II) ions should locate in the framework; otherwise, it would be difficult to rationalize such a pronounced effect of the presence of Ni(II) ions on the decomposition temperature of the organic linkers.¹⁵

SEM and EDS Study. SEM images of undoped and doped MOF-5s are obtained and shown in Figure 3. The pure MOF-5 morphology is characterized by well-defined cubic crystals of 50–200 μm in width. Ni-doped MOF-5s show very similar features, suggesting that Ni-doping does not change the morphology of MOF-5.

The EDS mappings of the Ni-doped MOF-5s were measured to study the dispersity of Ni(II) ions, as shown in Figure 4. The SEM images completely correspond to the images of the EDS

mapping of Zn and Ni. The Zn mapping follows the structure of MOF-5 crystals, and the Ni mapping is consistent with Zn mapping, suggesting that Ni(II) ions are well dispersed in the MOF-5 crystals. Compared to Ni13-MOF-5 (Figure 4a), the Ni mapping of Ni22-MOF-5 (Figure 4b) shows stronger intensity, indicating the higher content of Ni elements. The EDS plots of Ni-doped MOF-5s exhibit the signals of carbon $K\alpha$ (0.277 keV), oxygen $K\alpha$ (0.523 keV), zinc $K\alpha$ (1.012 keV), and nickel $K\alpha$ (0.952 keV) (Figure 5). The EDS results also give that the average atomic ratios of Ni to Zn in Ni13-MOF-5 and Ni22-MOF-5 are 0.15:1 and 0.33:1, respectively, consistent with the ICP and AAS analysis.

DRUV–Vis Spectra Analysis. The activation of MOF materials is a very important step before gas sorption measurement. Generally, high-temperature and long-time heating under vacuum will remove the guest molecules of the solvent-exchanged MOFs more completely. However, these always destroy the framework during the guest removing process when the temperature is too high and/or the time is too long, depending on the stability of the framework. How to indicate the proceeding of the activation process is still a big challenge nowadays. In our study, it is interesting to observe the color change phenomena during the activation process. The colors of Ni-doped MOF-5s are basically light green and gradually deepen with the contents of nickel increasing. When the chloroform-exchanged Ni-doped MOF-5s were degassed at 120 °C for 12 h on degassing station, colors change from pea green to purple, as shown in Figure 6. The same process of

Table 2. N₂, Ar, and H₂ Adsorption Properties of MOF-5s

samples	N ₂ /77 K		Ar/87 K		pore width ^c (nm)	V(H ₂) ^d (cm ³ /g)	H ₂ uptake ^d (wt %)
	B-SSA ^a /L-SSA ^b (m ² /g)	pore vol ^c (cm ³ /g)	B-SSA ^a /L-SSA ^b (m ² /g)	pore vol ^c (cm ³ /g)			
MOF-5-DEF ¹²	2750/–	1.15				160	1.44
MOF-5	1153.0/1224.5	0.518	1101.5/1119.5	0.611	0.582	198	1.78
Ni13-MOF-5	2699.0/2867.9	1.105	3630.1/4020.0	1.418	1.251	159	1.43
Ni22-MOF-5	2854.8/3032.6	1.111	3805.1/4145.8	1.466	1.251	150	1.35
MOF-5-DEF-d ¹²						0	0
MOF-5-4d						10.6	0.01
Ni13-MOF-5-4d						109	0.98
Ni22-MOF-5-4d						137	1.23

^aB-SSA = BET surface area. ^bLangmuir surface area. ^cDetermined by NLDFT pore size distribution. ^dMaximum uptake observed at 77 K.

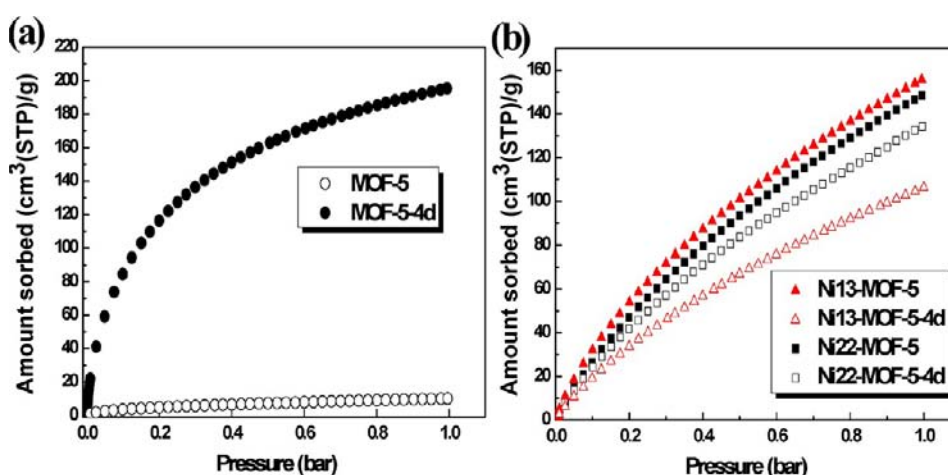


Figure 8. Hydrogen uptake capacities of (a) MOF-5 and (b) Ni-doped MOF-5 before and after 4 days exposure to ambient air.

pure white MOF-5 did not show clear color change even after 12 h evacuation in vacuum. It is noted that the colors of the activated MOF-5s show the complementary colors (blue-violet for Ni13-MOF-5 and fuchsia for Ni22-MOF-5) of the unactivated MOF-5s, which is a clear indication for the activation. DRUV-vis spectra were further performed to confirm color change phenomena. The absorption peaks in Figure 6b–d are consistent with their colors. The spectra of Ni-doped MOFs display two strong bands (420 and 720 nm), which strongly resembles the structure of Ni(II) complex where Ni(II) is in an octahedral coordination.¹⁷ The spectra of the evacuated Ni-doped MOF-5s (the purple color) exhibit three bands (440, 520, and 610 nm), which are related to the structure of [NiX₄]²⁻.¹⁸ Moreover, if the dehydrated Ni-doped MOF-5s are exposed to air or CHCl₃, the light green color would be recovered and the DRUV-vis spectra also come back, indicating that the coordination environment of Ni(II) ion could undergo reversible change. Recently, Mircea Dinca's work suggested that Zn₃O(carboxylate)₆ SBU of MOF-5 can serve as a tripodal chelating ligand to stabilize both tetrahedral and octahedral Ni(II) ions, confirmed by *in situ* diffuse-reflectance spectra and magnetic susceptibility study. This interesting result, as well as our work, clearly demonstrates that Ni(II) ion can replace Zn(II) ion to form a new analogue of MOF-5.¹⁹

Gas Sorption Analysis. To evaluate the influence of Ni-doping on the permanent porosity of the samples, N₂ and Ar sorption isotherms at 77 and 87 K were measured, respectively (Figure 7). The specific surface area (SSA) of undoped MOF-5

is 1153.0 and 1224.5 m² g⁻¹, obtained by using the multipoint BET and the Langmuir equations at 77 K, respectively. It is interesting that Ni-doping increases Langmuir specific surface areas (L-SSA) to 2867.9 and 3032.6 m² g⁻¹ for Ni13-MOF-5 and Ni22-MOF-5, respectively. The L-SSA of our synthesized MOF-5 is close to the values of the interpenetrated MOF-5 materials (600–2500 m² g⁻¹) obtained from dimethylformamide (DMF) solutions, but lower than the value of MOF-5 materials (3100–4000 m² g⁻¹) obtained from diethylformamide (DEF) solutions.^{13,14,20–22} The low SSA of MOF-5 material of this work is due to the interpenetrated structure.¹⁴ Furthermore, the BET and SSA of Ni22-MOF-5 from Ar sorption isotherm are 3805.1 and 4145.8 m² g⁻¹, respectively, which are larger than that from N₂ sorption isotherm (Table 2), mainly because the monatomic molecule Ar can enter the pores more compact than the diatomic molecule N₂. Ni22-MOF-5 shows to date one of the highest L-SSAs for DMF solvent-based MOF-5s, which is close to the reported 4400 m² g⁻¹ of DEF solvent-based MOF-5s.¹⁰ Therefore, DMF could be employed as a less costly alternative to DEF, which is significant for the commercial production of MOF-5. The result also suggests that Ni-doping may prevent inducing zinc species into the structure and the interpenetration of the frameworks.

The pore size distributions (PSDs) of MOF-5s were obtained by applying nonlocal density functional theory (NLDFT) with Ar (87.5 K) zeolite kernel based on a cylindrical pore model (Figure 7c). The PSDs of undoped MOF-5 exhibit a main narrow pore size distribution centered around 0.582 nm, and a few around 1.251 nm, according with

the a majority of interpenetrated structure.¹⁴ The PSDs of Ni-doped MOF-5s are mainly around 1.251 nm, especially when the doping amount increased to 22%, indicating that the interpenetrated structures in the Ni-doped MOF-5s are very little.

The H₂ adsorption behaviors of MOF-5 and Ni-doped MOF-5s at 77 K are shown in Figure 8 and Table 2. The H₂ uptake capacity of MOF-5 is 1.78 wt %, consistent with the value of the interpenetrated MOF-5.^{16b} Ni-doped MOF-5s demonstrate lower hydrogen uptake capacities (1.43 wt % for Ni13-MOF-5 and 1.35 wt % for Ni22-MOF-5). However, these values are very close to that of the typical MOF-5 materials,^{12,23} further proving the absence of the interpenetrated structure in our MOF-5s.

The isosteric heat of adsorption (Q_{st}) was calculated from the adsorption isotherms at 77 and 87 K using both Clausius–Clapeyron equation and virial-type fitting to quantitatively evaluate the binding strengths between hydrogen and the frameworks (Figure 9).²⁴ The Q_{st} values at low coverage are 8.9

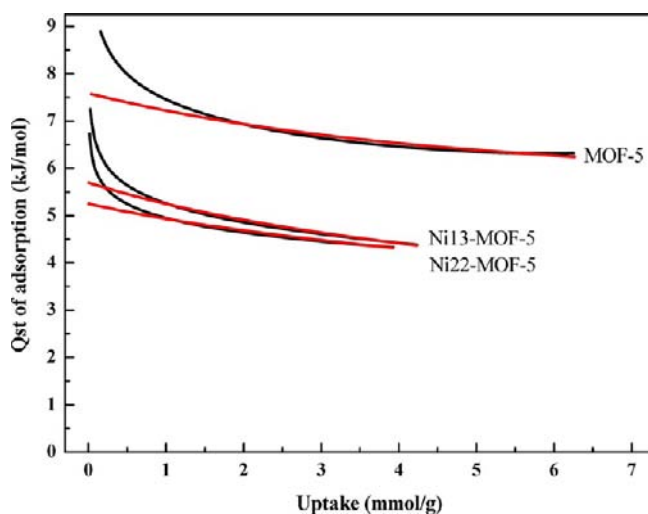


Figure 9. Isosteric heats of H₂ adsorption (Q_{st}) values for MOF-5, Ni13-MOF-5, and Ni22-MOF-5. The black and red lines are estimated by Clausius–Clapeyron equation and virial-type fitting, respectively.

kJ mol^{-1} calculated by Clausius–Clapeyron equation and 7.6 kJ mol^{-1} estimated by virial-type fitting for MOF-5; comparably high values have also been found in MOF-5 materials,^{10,15,23,25} providing further evidence that H₂ interacts more strongly in the appropriate small pores, and in agreement with its high hydrogen absorption capacity. Furthermore, the Q_{st} values of adsorption at low coverage are 7.3 and 6.7 kJ mol^{-1} calculated by Clausius–Clapeyron equation, and 5.7 and 5.3 kJ mol^{-1} estimated by virial-type fitting for Ni13-MOF-5 and Ni22-MOF-5, respectively. To the best of our knowledge, no DEF solvent-based MOF-5s without interpenetration showing similar SSAs and pores have been reported so far with higher Q_{st} of H₂.^{10,15,23,25a}

Of significant interest is the hydrogen storage uptake capability of Ni-doped MOF-5s after exposure to ambient air. It is well documented that MOF-5 completely loses its hydrogen storage capability after exposure to ambient air due to the collapse of the framework structure within 4 days, which is consistent with our result (Figure 8a).¹² However, the hydrogen uptake capacities of Ni-doped MOF-5s (Ni13-MOF-

5-4d and Ni22-MOF-5-4d) can be recovered after exposure to ambient air four days with a relative humidity of 30–37%. Before each measurement, Ni13-MOF-5-4d and Ni22-MOF-5-4d were reactivated by heating the samples at 120 °C in vacuum for 12 h. The hydrogen uptake capacity of Ni13-MOF-5-4d is reduced to 0.98 wt % exposure to ambient air, whereas the hydrogen adsorption of Ni22-MOF-5-4d remains 1.23 wt %. These results, again, imply that Ni-doping plays an important role for enhancing the hydrostability of MOF-5 materials. This result could possibly be due to the hydrostability of Ni_x(Zn)_{4-x}O⁶⁺ cluster SBU is more stable than Zn₄O⁶⁺ cluster SBU.²⁶

CONCLUSIONS

In conclusion, partial doping of the MOF-5 framework with Ni(II) ions has been successfully carried out. The isomorphous substitutions were achieved during crystallization in the synthesis procedure. The Ni-doped MOF-5s show higher SSA and larger pores than the undoped interpenetrated MOF-5, implying Ni-doping can prevent inducing zinc species into the framework and the interpenetrated structure. This study opens a new approach to enhance the hydrostability of MOFs, and thus gives a better retention ability of gas storage abilities when exposed to ambient air, as well as for other potential applications such as in the fields of catalysis and semiconductor materials.

AUTHOR INFORMATION

Corresponding Author

*E-mail: pcheng@nankai.edu.cn (P.C.); shiwei@nankai.edu.cn (W.S.).

Notes

The authors declare no competing financial interest.

ACKNOWLEDGMENTS

We thank the “973 Program” (2012CB821702), the NSFC (90922032, 20971073, and 21171100), the NSF of Tianjin (09JCZDJC22100), and MOE (20100031110009 and IRT0927).

REFERENCES

- (1) (a) Schlögl, L.; Züttel, A. *Nature* **2001**, *414*, 353–358. (b) Morris, R. E.; Wheatley, P. S. *Angew. Chem., Int. Ed.* **2008**, *47*, 4966–4981.
- (2) (a) Grochala, W.; Edwards, P. P. *Chem. Rev.* **2004**, *104*, 1283–1315. (b) Eberle, U.; Felderhoff, M.; Schuth, F. *Angew. Chem., Int. Ed.* **2009**, *48*, 6608–6630.
- (3) (a) Larsen, W. R.; Wojtas, L.; Perman, J.; Musselman, R. L.; Zaworotko, M. J.; Vrombale, C. M. *J. Am. Chem. Soc.* **2011**, *133*, 10356–10359. (b) Farha, O. K.; Spokoyny, A. M.; Mulfort, K. L.; Hawthorne, M. F.; Mirkin, C. A.; Hupp, J. T. *J. Am. Chem. Soc.* **2007**, *129*, 12680–12681. (c) Farha, O. K.; Hupp, J. T. *Acc. Chem. Res.* **2010**, *43*, 1166–1175. (d) Pan, L.; Sander, M. B.; Huang, X. Y.; Li, J.; Smith, M.; Bittner, E.; Bockrath, B.; Johnson, J. K. *J. Am. Chem. Soc.* **2004**, *126*, 1308–1309. (e) Ong, T. T.; Kavuru, P.; Nguyen, T.; Cantwell, R.; Wojtas, L.; Zaworotko, M. J. *J. Am. Chem. Soc.* **2011**, *133*, 9224–9227. (f) Banerjee, M.; Das, S.; Yoon, M.; Choi, H. J.; Hyun, M. H.; Park, S. M.; Seo, G.; Kim, K. *J. Am. Chem. Soc.* **2009**, *131*, 7524–7525. (g) Meek, S. T.; Greathouse, J. A.; Allendorf, M. D. *Adv. Mater.* **2011**, *23*, 249–267.
- (4) (a) Yaghi, O. M.; Li, G.; Li, H. *Nature* **1995**, *378*, 703–706. (b) Chen, B.; Eddaoudi, M.; Hyde, S. T.; O’Keeffe, M.; Yaghi, O. M. *Science* **2001**, *291*, 1021–1023. (c) Murray, L. J.; Dinca, M.; Long, J. R. *Chem. Soc. Rev.* **2009**, *38*, 1294–1314. (d) Ma, S.; Zhou, H.-C. *J. Am. Chem. Soc.* **2009**, *131*, 1294–1314.

- Chem. Soc.* **2006**, *128*, 11734–11735. (e) Matsuda, R.; Kitaura, R.; Kitagawa, S.; Kubota, Y.; Belosludov, R. V.; Kobayashi, T. C.; Sakamoto, H.; Chiba, T.; Takata, M.; Kawazoe, Y.; Mita, Y. *Nature* **2005**, *436*, 238–241. (f) Kesanli, B.; Cui, Y.; Smith, M.; Bittner, E.; Bockrath, B.; Lin, W. *Angew. Chem., Int. Ed.* **2004**, *44*, 72–75. (g) Zhuang, W.; Yuan, D.; Liu, D.; Zhong, C.; Li, J.-R.; Zhou, H.-C. *Chem. Mater.* **2012**, *24*, 18–25.
- (5) (a) Eddaoudi, M.; Kim, J.; Vodak, D.; Wachter, J.; O’Keeffe, M.; Yaghi, O. M. *Science* **2002**, *295*, 469–472. (b) Hayashi, H.; Côté, A. P.; Furukawa, H.; O’Keeffe, M.; Yaghi, O. M. *Nat. Mater.* **2007**, *6*, 501–506. (c) Li, J.-R.; Kuppler, R. J.; Zhou, H.-C. *Chem. Soc. Rev.* **2009**, *38*, 1477–1504. (d) Kuppler, R. J.; Timmons, D. J.; Fang, Q. R.; Li, J. R.; Makal, T. A.; Young, M. D.; Yuan, D. Q.; Zhao, D.; Zhuang, W. J.; Zhou, H. C. *Coord. Chem. Rev.* **2009**, *253*, 3042–3066. (e) Demessence, A.; D’Alessandro, D. M.; Foo, M. L.; Long, J. R. *J. Am. Chem. Soc.* **2009**, *131*, 8784–8786. (f) Horcajada, P.; Serre, C.; Sebban, M.; Taulelle, F.; Férey, G. *Angew. Chem., Int. Ed.* **2006**, *45*, 5974–5978. (g) Zhao, X. B.; Xiao, B.; Fletcher, A. J.; Thomas, K. M.; Bradshaw, D.; Rosseinsky, M. J. *Science* **2004**, *306*, 1012–1015.
- (6) (a) Hasegawa, S.; Horike, S.; Matsuda, R.; Furukawa, S.; Mochizuki, K.; Kinoshita, Y.; Kitagawa, S. *J. Am. Chem. Soc.* **2007**, *129*, 2607–2614. (b) Corma, A.; Garcia, H.; Llabrés i Xamena, F. X. *Chem. Rev.* **2010**, *110*, 4606–4655. (c) Lee, J. Y.; Farha, O. K.; Roberts, J.; Scheidt, K. A.; Nguyen, S. T.; Hupp, J. T. *Chem. Soc. Rev.* **2009**, *38*, 1450–1459. (d) Fujita, M.; Kwon, Y. J.; Washizu, S.; Ogura, K. *J. Am. Chem. Soc.* **1994**, *116*, 1151–1152. (e) Seo, J. S.; Whang, D.; Lee, H.; Jun, S. I.; Oh, J.; Jeon, Y. J.; Kim, K. *Nature* **2000**, *404*, 982–986. (f) Wu, C. D.; Hu, A.; Zhang, L.; Lin, W. B. *J. Am. Chem. Soc.* **2005**, *127*, 8940–8941. (g) Serra-Crespo, P.; Ramos-Fernandez, E. V.; Gascon, J.; Kapteijn, F. *Chem. Mater.* **2011**, *23*, 2565–2572.
- (7) (a) Allendorf, M. D.; Bauer, C. A.; Bhakta, R. K.; Houk, R. J. T. *Chem. Soc. Rev.* **2009**, *38*, 1330–1352. (b) MasPOCH, D.; Ruiz-Molina, D.; Veciana, J. *Chem. Soc. Rev.* **2007**, *36*, 770–818. (c) Suh, M. P.; Cheon, Y. E.; Lee, E. Y. *Coord. Chem. Rev.* **2008**, *252*, 1007–1026. (d) Cui, Y.; Yue, Y.; Qian, G.; Chen, B. *Chem. Rev.* **2012**, *112*, 1126–1162. (e) Beauvais, L. G.; Shores, M. P.; Long, J. R. *J. Am. Chem. Soc.* **2000**, *122*, 2763–2772. (f) Albrecht, M.; Lutz, M.; Spek, A. L.; van Koten, G. *Nature* **2000**, *406*, 970–974. (g) Real, J. A.; Andrss, E.; MuToz, M. C.; Julve, M.; Granier, T.; Bousseksou, A.; Varret, F. *Science* **1995**, *268*, 265–267.
- (8) Rosi, N. L.; Eckert, J.; Eddaoudi, M.; Vodak, D. T.; Kim, J.; O’Keeffe, M.; Yaghi, O. M. *Science* **2003**, *300*, 1127–1129.
- (9) (a) Li, H.; Eddaoudi, M.; O’Keeffe, M.; Yaghi, O. M. *Nature* **1999**, *402*, 276–279. (b) Panella, B.; Hirscher, M. *Adv. Mater.* **2005**, *17*, 538–541. (c) Rowsell, J. L. C.; Milward, A. R.; Park, K. S.; Yaghi, O. M. *J. Am. Chem. Soc.* **2004**, *126*, 5666–5667. (d) Rowsell, J. L. C.; Eckert, J.; Yaghi, O. M. *J. Am. Chem. Soc.* **2005**, *127*, 14904–14910. (e) Li, Y.; Yang, R. T. *J. Am. Chem. Soc.* **2006**, *128*, 8136–8137. (f) Sillar, K.; Hofmann, A.; Sauer, J. *J. Am. Chem. Soc.* **2009**, *131*, 4143–4150.
- (10) Kaye, S. S.; Dailly, A.; Yaghi, O. M.; Long, J. R. *J. Am. Chem. Soc.* **2007**, *129*, 14176–14177.
- (11) Greathouse, J. A.; Allendorf, M. D. *J. Am. Chem. Soc.* **2006**, *128*, 10678–10679.
- (12) Yang, J.; Grzech, A.; Mulder, F. M.; Dingemans, T. J. *Chem. Commun.* **2011**, *47*, 5244–5246.
- (13) Yang, S. J.; Choi, J. Y.; Chae, H. K.; Cho, J. H.; Nahm, K. S.; Park, C. R. *Chem. Mater.* **2009**, *21*, 1893–1897.
- (14) Hafizovic, J.; Bjorgen, M.; Olsbye, U.; Dietzel, P. D. C.; Bordiga, S.; Prestipino, C.; Lamberti, C.; Lillerud, K. P. *J. Am. Chem. Soc.* **2007**, *129*, 3612–3620.
- (15) Botas, J. A.; Calleja, G.; Sánchez-Sánchez, M.; Orcajo, M. G. *Langmuir* **2010**, *26*, 5300–5303.
- (16) (a) Hausdorf, S.; Wagler, J.; Mossig, R.; Mertens, F. O. R. L. *J. Phys. Chem. A* **2008**, *112*, 7567–7576. (b) Chen, B.; Wang, X.; Zhang, Q.; Xi, X.; Cai, J.; Qi, H.; Shi, S.; Wang, J.; Yuan, D.; Fang, M. *J. Mater. Chem.* **2010**, *20*, 3758–3767. (c) Nguyen, J. G.; Cohen, S. M. *J. Am. Chem. Soc.* **2010**, *132*, 4560–4561.
- (17) Wells, A. F. *Structural Inorganic Chemistry*; Oxford Press: Oxford, U.K., 1984.
- (18) Zheng, B. N.; Miranda, M. O.; DiPasquale, A. G.; Golen, J. A.; Rheingold, A. L.; Doerr, L. H. *Inorg. Chem.* **2009**, *48*, 4274–4276.
- (19) Brozek, C. K.; Dinca, M. *Chem. Sci.* **2012**, *3*, 2110–2113.
- (20) Huang, L.; Wang, H.; Chen, J.; Wang, Z.; Sun, J.; Zhao, D.; Yan, Y. *Microporous Mesoporous Mater.* **2003**, *58*, 105–114.
- (21) Tsao, C.-S.; Yu, M.-S.; Chung, T.-Y.; Wu, H.-C.; Wang, C.-Y.; Chang, K.-S.; Chen, H.-L. *J. Am. Chem. Soc.* **2007**, *129*, 15997–16004.
- (22) Grzesiak, A. L.; Uribe, F. J.; Ockwig, N. W.; Yaghi, O. M.; Matzger, A. J. *Angew. Chem., Int. Ed.* **2006**, *45*, 2553–2556.
- (23) Rowsell, J. L. C.; Yaghi, O. M. *J. Am. Chem. Soc.* **2006**, *128*, 1304–1315.
- (24) (a) Dincă, M.; Long, J. R. *J. Am. Chem. Soc.* **2005**, *127*, 9376–9377. (b) Dincă, M.; Dailly, A.; Liu, Y.; Brown, C. M.; Neumann, D. A.; Long, J. R. *J. Am. Chem. Soc.* **2006**, *128*, 16876–16883.
- (25) (a) Panella, B.; Hirscher, M.; Pütter, H.; Müller, U. *Adv. Funct. Mater.* **2006**, *16*, 520–524. (b) Xin, Z.; Bai, J.; Pan, Y.; Zaworotko, M. J. *Chem.—Eur. J.* **2010**, *16*, 13049–13052. (c) Kim, H.; Das, S.; Kim, M. G.; Dybtsev, D. N.; Kim, Y.; Kim, K. *Inorg. Chem.* **2011**, *50*, 3691–3696.
- (26) Low, J. J.; Benin, A. I.; Jakubczak, P.; Abrahamian, J. F.; Faheem, S. A.; Willis, R. R. *J. Am. Chem. Soc.* **2009**, *131*, 15834–15842.